

Transforming H&E images into IHC: A Variance-Penalized GAN for Precision Oncology

Sara Rehmat^{*§}, Hafeez Ur Rehman^{*†‡}

^{*} Department of Computer Science, National University of Computer and Emerging Sciences, Islamabad, Pakistan

[†] School of Computing and Data Science, Oryx Universal College with Liverpool John Moores University, Doha, Qatar

[‡] Corresponding Author; Email: hafeez.r@oryx.edu.qa, h.urrehman@ljmu.ac.uk, hafeez.urrehman@nu.edu.pk
[§] p218901@nu.edu.pk

Abstract—The overexpression of the human epidermal growth factor receptor 2 (HER2) in breast cells is a key driver of HER2-positive breast cancer, a highly aggressive subtype requiring precise diagnosis and targeted therapy. Immunohistochemistry (IHC) is the standard technique for HER2 assessment but is costly, labor-intensive, and highly dependent on antibody selection. In contrast, hematoxylin and eosin (H&E) staining, a routine histopathological procedure, offers broader accessibility but lacks HER2 specificity. This study proposes an advanced deep learning-based image translation framework to generate high-fidelity IHC images from H&E-stained tissue samples, enabling cost-effective and scalable HER2 assessment. By modifying the loss function of pyramid pix2pix, we mitigate mode collapse, a fundamental limitation in generative adversarial networks (GANs), and introduce a novel variance-based penalty that enforces structural diversity in generated images. Our model particularly excels in translating HER2-positive (IHC 3+) images, which have remained challenging for existing methods due to their complex morphological variations. Extensive evaluations on the BCI histopathological dataset demonstrate that our model surpasses state-of-the-art methods in terms of peak signal-to-noise ratio (PSNR), structural similarity index (SSIM), and Fréchet Inception Distance (FID), particularly in accurately translating HER2-positive (IHC 3+) images. Beyond medical imaging, our model exhibits superior performance in general image-to-image translation tasks, showcasing its potential across multiple domains. This work marks a significant step toward AI-driven precision oncology, offering a reliable and efficient alternative to traditional HER2 diagnostics.

Index Terms—breast cancer, HER2 cancer, image translation, GANs, mode collapse

I. INTRODUCTION

Breast cancer remains the most prevalent form of cancer worldwide [1]. Among its various subtypes, approximately 20% of the cases are classified as HER2-positive breast cancer, characterized by overexpression of the human epidermal growth factor receptor 2 (HER2) [2]. This subtype is particularly aggressive and requires targeted therapies, such as Herceptin, to inhibit HER2 signaling. However, accurate HER2 classification is critical, as misdiagnosis can lead to inappropriate treatment strategies and higher recurrence rates [3].

The gold standard for HER2 detection is fluorescence in situ hybridization (FISH), a molecular technique that assesses gene amplification [4]. However, FISH is costly, time consuming

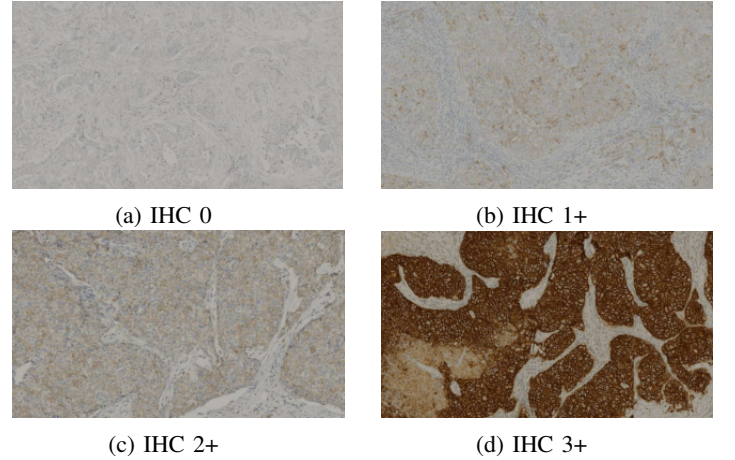


Fig. 1: Different types of IHC images based on levels of HER2 expression in the BCI dataset [10]. The higher the HER2 expression, the greater the corresponding label.

and not widely available in all clinical laboratories [5]. Immunohistochemistry (IHC) provides a more accessible alternative, relying on antibody-antigen interactions to detect HER2 expression [6], [7]. IHC results are categorized into four levels: 0, 1+, 2+, and 3+, as illustrated in Fig. 1. Although IHC 0 and 1+ are HER2-negative, IHC 3+ is strongly HER2-positive and indicates eligibility for HER2-targeted therapies. However, IHC 2+ remains ambiguous, necessitating additional FISH testing [2]. Despite its utility, IHC still requires specialized reagents, expensive equipment, and experienced pathologists for interpretation, introducing subjectivity in diagnosis [8], [9].

Hematoxylin and eosin (H&E) staining is the standard histopathological technique used for initial cancer screening. Unlike IHC, H&E is cost-effective, rapid, and independent of antibody selection, making it widely used for cancer diagnosis. H&E stains nuclei blue to dark purple and cytoplasm in various shades of pink and red, providing high-contrast images for structural analysis. Fig. 2 illustrates the three primary techniques used in HER2 detection: H&E, IHC, and FISH.

Recent advances in deep learning have demonstrated that H&E images alone can predict HER2 status without IHC [11]. Studies [12]–[16] have used convolutional neural networks (CNNs) and transformers to classify HER2 expression

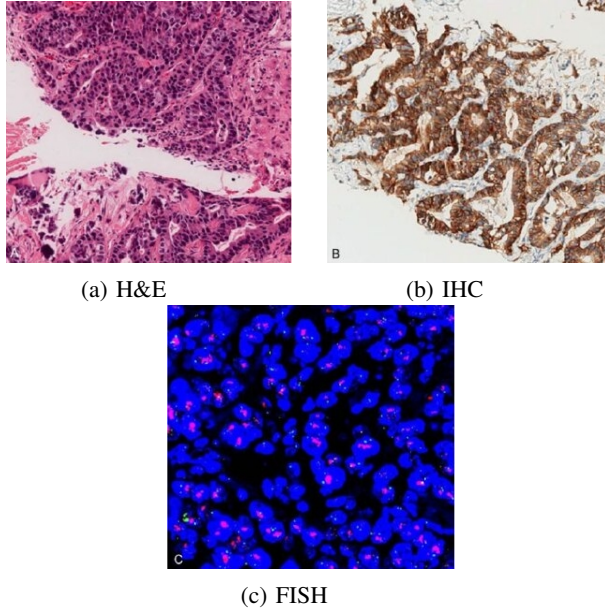


Fig. 2: Different techniques for HER2 detection. These patches are from whole-slide images of biopsied tissue samples treated using H&E (a), IHC (b), and FISH (c).

directly from H&E images. However, a direct H&E-based classification lacks interpretability, which limits its adoption in clinical practice. Instead, a more promising approach is to translate H&E images into IHC-like images, allowing human pathologist validation and dataset augmentation.

Liu *et al.* [10] pioneered this approach using a GAN-based pyramid pix2pix model, training it on their BCI dataset. While pyramid pix2pix improved image translation, it struggled to generate realistic IHC 3+ images, suffering from mode collapse, where the model fails to capture diverse HER2-positive morphologies. This limitation undermines the clinical utility of the generated IHC images, particularly for HER2-positive cases where a precise classification is required.

This work aims to address the shortcomings of existing image translation models and proposes a novel GAN-based framework with an enhanced loss function. By modifying the loss function, we mitigate mode collapse problem, a fundamental limitation in generative adversarial networks (GANs), and introduce a novel variance-based penalty that enforces structural diversity in generated images. Specifically, our work seeks to:

- 1) Improve the translation of H&E images into high-fidelity IHC images, particularly for HER2-positive (IHC 3+) cases, which remain a challenge for existing models.
- 2) Mitigate mode collapse by introducing a variance-based loss function, ensuring greater diversity in generated images.
- 3) Evaluate the generalizability of our model beyond medical imaging by testing it on generic image translation tasks.

To achieve these objectives, we introduce a variance penalty term into the loss function of the pyramid pix2pix model, enforcing structural diversity and fidelity in IHC image gener-

ation. Our model is rigorously evaluated using the BCI dataset for HER2 classification and LLVIP dataset for general image translation, demonstrating superior performance over existing approaches [17].

The remainder of this paper is structured as follows: Section II reviews existing research on breast cancer detection and image translation techniques. Section III outlines our proposed methodology. Section IV describes the experimental setup including the analysis of the dataset and the discussion of evaluation metrics we have used. Section V presents the comparative results, and Section VI concludes the study with insights on future research directions.

II. LITERATURE REVIEW

Breast cancer is among the most prevalent malignancies worldwide, requiring advanced techniques for early detection and classification. Significant research efforts have been devoted to automating breast cancer diagnosis using a combination of image processing, machine learning, and deep learning techniques. Traditional image processing methods have focused on nuclei segmentation and feature extraction to differentiate between malignant and benign tumors [18]. With the advent of machine learning, algorithms such as support vector machines (SVMs) and random forests have demonstrated high efficacy in breast cancer classification [19]–[21]. More recently, deep learning architectures, particularly convolutional neural networks (CNNs), have significantly enhanced histopathological image classification by automatically learning hierarchical representations [22]–[25].

The recent emergence of Vision Transformers (ViTs) [26] and their variants [27], [28] has further revolutionized the field. Unlike CNNs, which rely on localized receptive fields, ViTs utilize self-attention mechanisms to model long-range dependencies in images, leading to improved feature extraction and classification. Several studies have successfully deployed ViTs for breast cancer detection [29]–[33], demonstrating superior performance over traditional CNNs.

An important aspect of automated breast cancer diagnosis is the availability of high-quality datasets. The *BreakHis* dataset [34] is widely used in breast cancer classification, consisting of 9,109 microscopic images of benign and malignant tumors obtained at different magnifications. Additionally, the BreCaHAD (Breast Cancer Histopathological Annotation and Diagnosis) dataset [35] and the BACH (Breast Cancer Histology Challenge) dataset [36] provide rich sources of labeled histopathological images for benchmarking various computational models.

Beyond morphological classification, biomarker analysis plays a pivotal role in determining treatment strategies for breast cancer patients. Immunohistochemistry (IHC) is a widely used method to assess biomarkers such as estrogen receptors (ER), progesterone receptors (PR), and human epidermal growth factor receptor 2 (HER2), which guide targeted therapies. Recent studies [11]–[13] have demonstrated that machine learning algorithms can predict biomarker expression directly from hematoxylin and eosin (H&E)-stained images, highlighting a strong correlation between morphological structures in H&E images and biochemical properties observed

in IHC images. This has motivated researchers to explore the translation of H&E images into IHC images as a means to facilitate biomarker assessment while reducing costs and dependency on specialized laboratory techniques.

Image-to-image translation is a critical area of research in computational pathology, particularly for the transformation of H&E-stained images into IHC images. Liu *et al.* [10] pioneered this effort by introducing a supervised deep learning framework for H&E to IHC image translation. Broadly, image translation methods can be categorized into unsupervised and supervised approaches. Unsupervised translation models, such as CycleGAN [37], DualGAN [38], and UNIT (Unsupervised Image-to-Image Translation Network) [39], leverage cycle consistency losses to map images between domains without paired training data. However, these approaches often struggle with preserving fine-grained histopathological details. In contrast, supervised models utilize paired datasets to learn a direct mapping between input and target images, resulting in more precise translations.

Among the supervised image translation models, the pix2pix framework [40] introduced conditional generative adversarial networks (cGANs) for image-to-image translation. pix2pixHD [41] extended this approach to generate high-resolution images using coarse-to-fine generators and multi-scale discriminators. Building on these advancements, Liu *et al.* proposed pyramid pix2pix, an enhanced version of pix2pix tailored for translating H&E images into IHC images [10]. Their key contribution was the creation of the BCI dataset, a large-scale paired dataset of H&E and IHC images. While pyramid pix2pix improved translation quality for low HER2 expression levels (IHC 0/1+/2+), it failed to generate realistic IHC 3+ images, suffering from mode collapse, a common limitation in generative adversarial networks (GANs).

Addressing mode collapse remains a critical challenge in GAN-based image translation. Several techniques have been proposed to mitigate this issue, including Wasserstein GANs (WGANs) [42], spectral normalization [43], mode regularization [44], and self-attention mechanisms [45]. However, none of these strategies have been explicitly applied to the translation of H&E images into IHC images. This gap underscores the need for novel loss functions that penalize mode collapse while maintaining fidelity and structural diversity in generated IHC images.

Given these limitations, our study introduces an enhanced loss function that explicitly penalizes low-diversity image generation by incorporating a variance-based regularization term. By addressing mode collapse, our approach improves the quality and diversity of IHC 3+ image generation, thereby advancing computer-aided HER2 breast cancer diagnostics. The proposed methodology is not only specific to histopathological image translation but also demonstrates promising results for generic image-to-image translation tasks, extending its applicability beyond biomedical imaging.

III. PROPOSED METHODOLOGY

The transformation of hematoxylin and eosin (H&E) stained images into Immunohistochemistry (IHC) stained images is a

fundamental challenge in digital pathology. Accurate translation between these imaging modalities is essential for both diagnostic and prognostic applications. However, existing generative models, such as pyramid pix2pix [10], often suffer from mode collapse, leading to reduced variability in generated images and suboptimal generalization across various histopathological samples, especially in translating HER2-positive (IHC 3+) images.

To overcome these challenges, we propose an enhancement to the loss function of pyramid pix2pix framework by introducing a variance difference regularization term. The general framework of our approach is illustrated in Fig. 3. The proposed modification encourages diversity in generated images, while maintaining fidelity to the original IHC image distributions. By penalizing lower variance in generated images relative to the input images, the model's learning is driven to generate more diverse and realistic representations, thereby reducing mode collapse and improving translation accuracy.

A. Pyramid pix2pix Framework

Pyramid pix2pix is an advanced image-to-image translation model that introduces multi-scale loss computation to mitigate misalignment issues present in the BCI dataset. The original objective function of pyramid pix2pix is defined as:

$$G^* = \arg \min_G \max_D \mathcal{L}_{\text{cGAN}}(G, D) + \lambda \mathcal{L}_1 + \mathcal{L}_{\text{multiscale}} \quad (1)$$

where $\mathcal{L}_{\text{cGAN}}$ represents the adversarial loss, \mathcal{L}_1 is the pixel-wise loss, and $\mathcal{L}_{\text{multiscale}}$ accounts for structural consistency across scales.

The adversarial loss $\mathcal{L}_{\text{cGAN}}$ is given by:

$$\mathcal{L}_{\text{cGAN}}(G, D) = \mathbb{E}[\log D(x, y)] + \mathbb{E}[\log(1 - D(x, G(x, z)))] \quad (2)$$

where z denotes a random noise vector, x is the H&E image, y is the corresponding IHC image, and $G(x, z)$ is the generated output. The discriminator D aims to classify real image pairs correctly, while the generator G seeks to fool D by generating realistic images.

The L1 loss enforces pixel-wise similarity and is expressed as:

$$\mathcal{L}_1(G) = \mathbb{E}_{x,y,z} [|y - G(x, z)|] \quad (3)$$

Additionally, the multi-scale loss $\mathcal{L}_{\text{multiscale}}$ is computed as:

$$\mathcal{L}_{\text{multiscale}}(G) = \sum_i \lambda_i S_i \quad (4)$$

where S_i represents structural differences computed at different scales:

$$S_i(G) = \mathbb{E}_{x,y,z} [|F_i(y) - F_i(G(x, z))|] \quad (5)$$

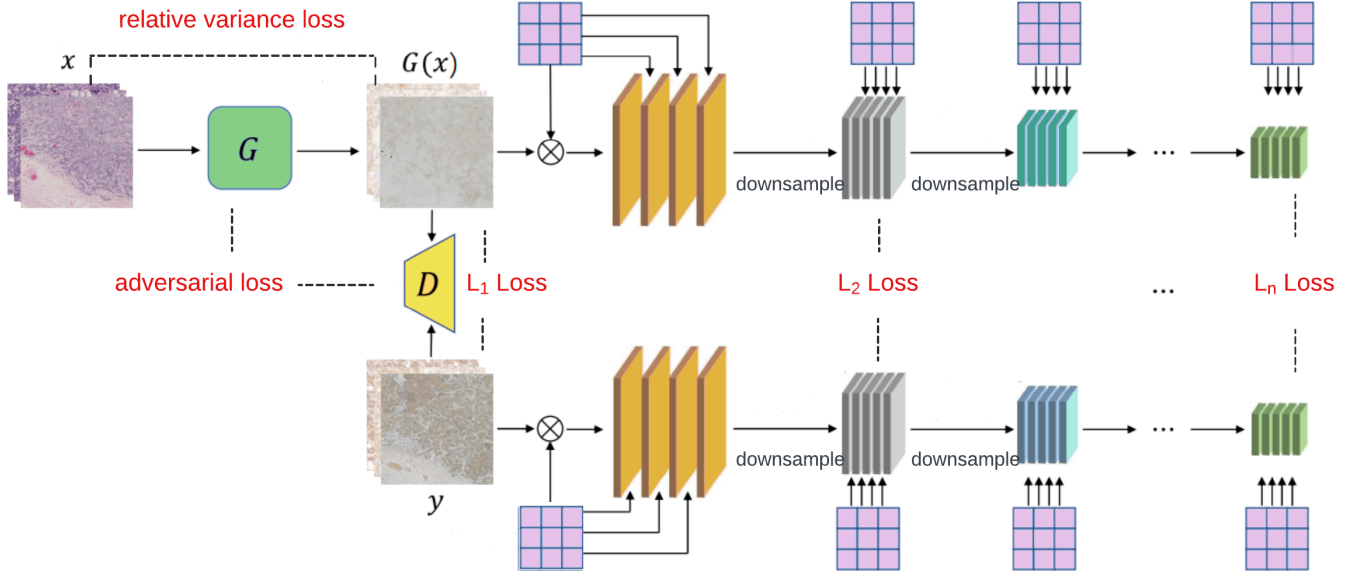


Fig. 3: The framework of the proposed architecture for generating high-fidelity IHC images from H&E images. The relative variance between input images and generated images in a batch is incorporated into the overall loss of pyramid pix2pix [10].

B. Variance-Based Loss for Mode Collapse Mitigation

One of the key challenges in generative models is mode collapse, where the generator produces limited variations of output images. To address this issue, we introduce a variance-based regularization term that penalizes low variance in generated images. The variance computation is performed across a batch of n images with C channels, height H , and width W .

First, the mean pixel value at each channel and spatial location is calculated as:

$$\mu(c, i, j) = \frac{1}{n} \sum_{k=1}^n f_{k,c,i,j} \quad (6)$$

The variance at each position across the batch is then computed as:

$$\sigma^2(c, i, j) = \frac{1}{n} \sum_{k=1}^n (f_{k,c,i,j} - \mu(c, i, j))^2 \quad (7)$$

Averaging over all pixels and channels, we obtain the overall variance:

$$\overline{\sigma^2} = \frac{1}{C \cdot H \cdot W} \sum_{c=1}^C \sum_{i=1}^H \sum_{j=1}^W \sigma^2(c, i, j) \quad (8)$$

Let $\overline{\sigma^2(f)}$ and $\overline{\sigma^2(G(f))}$ denote the variance of real and generated images, respectively. The variance difference is then defined as:

$$\Delta\sigma^2 = \left| \overline{\sigma^2(f)} - \overline{\sigma^2(G(f))} \right| \quad (9)$$

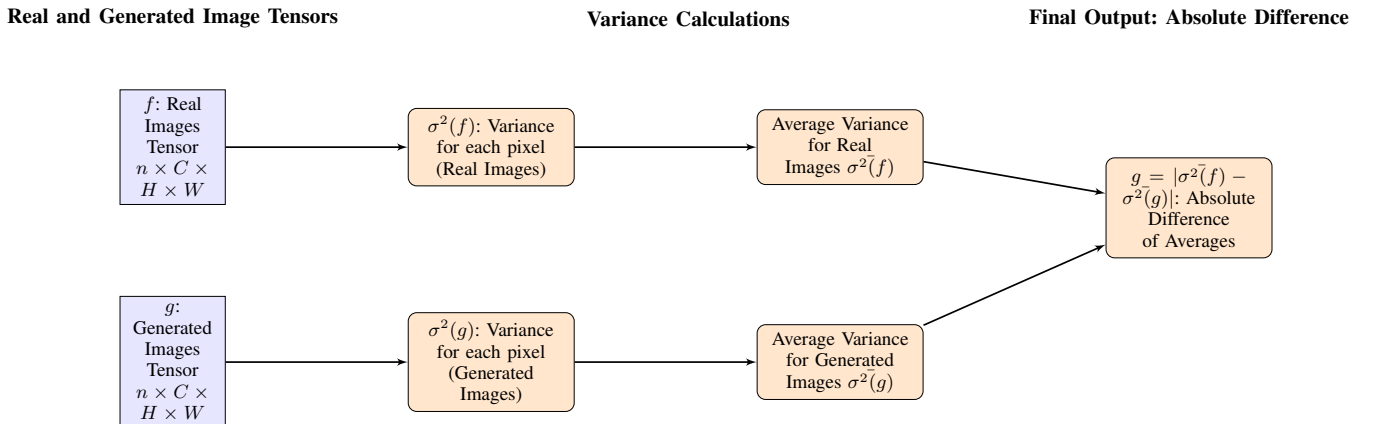


Fig. 4: Tensor operations and variance calculations for real and generated images.

This variance regularization term ensures that the generator maintains diversity in generated outputs. Fig. 4 illustrates the tensor operations involved in computing variance.

C. Final Objective Function

By incorporating the variance-based regularization term defined in equation 9 into the pyramid pix2pix loss function, we obtain the following final objective function:

$$G^* = \arg \min_G \max_D \mathcal{L}_{cGAN}(G, D) + \lambda \mathcal{L}_1 + \mathcal{L}_{\text{multiscale}} + \Delta \sigma^2 \quad (10)$$

The inclusion of $\Delta \sigma^2$ mitigates mode collapse by encouraging variance in generated images while maintaining structural consistency.

IV. EXPERIMENTAL SETUP

To evaluate the effectiveness of our proposed variance-based loss enhancement in pyramid pix2pix, we conduct experiments on a publicly available dataset [10] of paired hematoxylin and eosin (H&E) and Immunohistochemistry (IHC) stained images. The dataset comprises high-resolution histopathological images from multiple tissue samples, ensuring diversity in staining patterns and structural variations. We preprocess all images by normalizing intensity values and resizing them to a fixed resolution suitable for deep learning models. The training and validation splits are maintained at an 80:20 ratio to ensure a balanced evaluation. Our experiments are implemented using PyTorch and executed on Google Colab, leveraging its Tesla T4 GPU acceleration. The model is trained with a batch size of 8, an initial learning rate of 0.0002, and the Adam optimizer to ensure stable convergence.

A. Dataset Analysis

The BCI dataset curated by [10] serves as a comprehensive resource specifically designed for histopathological image translation tasks. It comprises 4873 paired image patches extracted from whole slide images of 51 patients, covering a broad spectrum of histological variations. The dataset includes all four categories of HER2 expression in IHC images: 0, 1+, 2+, and 3+. Each patch has a high resolution of 1024 x 1024 pixels, preserving fine-grained histopathological details necessary for accurate image-to-image translation. The paired nature of the dataset makes it particularly suitable for supervised learning approaches, where each H&E-stained image is directly associated with a corresponding IHC counterpart, as illustrated in Fig. 5.

The dataset exhibits a non-uniform distribution of IHC image patches across the four HER2 expression levels, reflecting real-world prevalence and variability in HER2 staining patterns. As depicted in Fig. 6, a higher proportion of images correspond to IHC 2+ expression, which represents a critical threshold category that requires additional FISH confirmation in clinical settings. The diversity of samples within the dataset is helpful in training models that can generalize effectively across different staining intensities and cellular morphologies. The variation in sample representation highlights the necessity

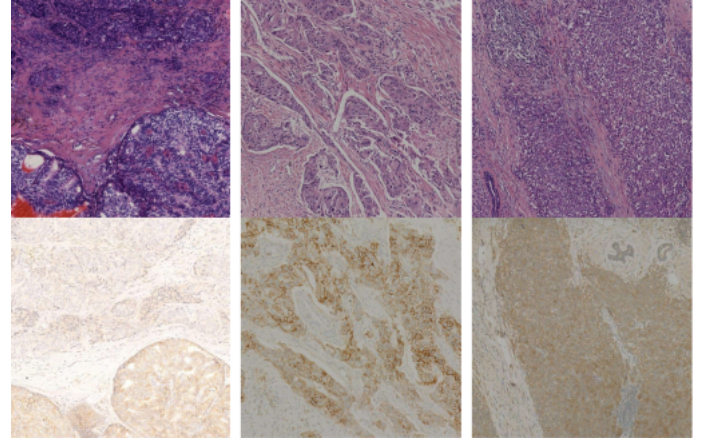


Fig. 5: Representative image patches from the BCI dataset [10], showcasing hematoxylin and eosin (H&E) stained images alongside their corresponding immunohistochemistry (IHC) images. The dataset provides paired samples for deep learning-based image translation and biomarker assessment.

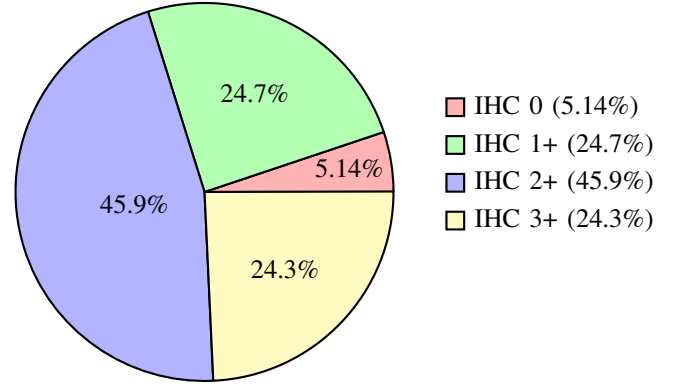


Fig. 6: Distribution of HER2 expression levels in the BCI dataset. The dataset is predominantly composed of IHC 2+ images, reflecting clinical scenarios where further fluorescence in situ hybridization (FISH) confirmation is required.

of developing robust translation models capable of accurately generating high-quality IHC images, even for underrepresented categories.

A detailed analysis of the dataset reveals significant variability in terms of color distribution, sharpness, and dynamic range across different HER2 expression levels. Fig. 7 illustrates differences in the average color means, highlighting distinct staining properties among different categories. Similarly, Fig. 8 and Fig. 9 provide insights into the texture and contrast variations between H&E and IHC images. These differences present challenges for existing generative models, particularly in maintaining structural integrity while ensuring realistic color translation. Addressing these variations remains essential for improving the fidelity of generated IHC images and enhancing their applicability in clinical diagnostic workflows.

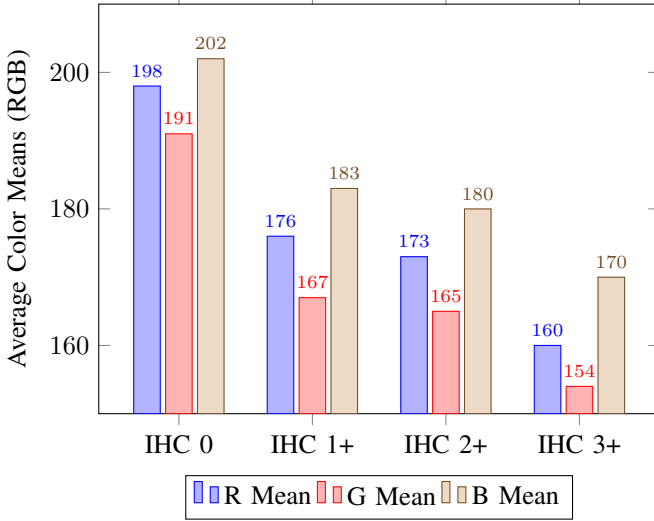


Fig. 7: Mean RGB color values for different HER2 expression levels in the BCI dataset. Distinct color variations highlight staining intensity differences across IHC categories.

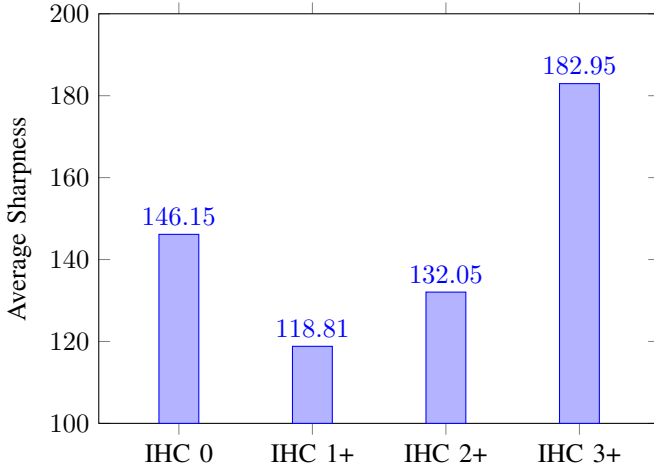


Fig. 8: Average sharpness values for different HER2 expression levels. The variability in sharpness reflects structural and textural differences among IHC categories, influencing diagnostic precision.

B. Evaluation Metrics

To assess the quality of the generated immunohistochemistry (IHC) images from hematoxylin and eosin (H&E) stained images, we employ three widely used evaluation metrics: Peak Signal-to-Noise Ratio (PSNR), Structural Similarity Index (SSIM) [46], and Fréchet Inception Distance (FID) [47]. Each of these metrics provides a complementary perspective on the accuracy and perceptual quality of the translated images.

1) *Peak Signal-to-Noise Ratio (PSNR)*: PSNR is a full-reference metric that quantifies the pixel-wise fidelity of the generated image with respect to the ground truth image. It is derived from the Mean Squared Error (MSE), which measures the pixel-wise difference between the original and generated images. Given an original image I and a reconstructed image K of size $m \times n$, the MSE is computed as:

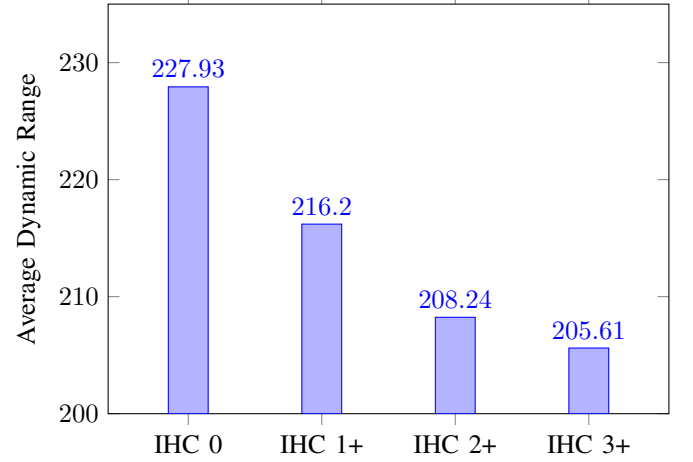


Fig. 9: Comparison of dynamic range values across HER2 expression levels. The decreasing trend in dynamic range correlates with increased HER2 expression, impacting the contrast in generated IHC images.

$$\text{MSE} = \frac{1}{mn} \sum_{i=0}^{m-1} \sum_{j=0}^{n-1} [I(i, j) - K(i, j)]^2. \quad (11)$$

Using MSE, PSNR is then calculated as:

$$\text{PSNR} = 10 \log_{10} \left(\frac{L^2}{\text{MSE}} \right), \quad (12)$$

where L is the maximum possible pixel value of the image (e.g., 255 for 8-bit images). Higher PSNR values indicate greater similarity between the generated and ground truth images, signifying lower reconstruction error. In the context of HE to IHC translation, PSNR provides an objective measure of how closely the pixel intensities in the generated IHC image match the real IHC counterpart. However, since PSNR does not account for perceptual quality and structural differences, it is best used in conjunction with other metrics.

2) *Structural Similarity Index (SSIM)*: SSIM is designed to model human visual perception by evaluating luminance, contrast, and structural similarity between the generated and ground truth images. Unlike PSNR, which only considers absolute differences, SSIM assesses structural distortions, which are crucial in medical image translation tasks where fine morphological details must be preserved. SSIM is computed as:

$$\text{SSIM}(x, y) = \frac{(2\mu_x\mu_y + C_1)(2\sigma_{xy} + C_2)}{(\mu_x^2 + \mu_y^2 + C_1)(\sigma_x^2 + \sigma_y^2 + C_2)}, \quad (13)$$

where:

- μ_x is the mean intensity of image x ,
- μ_y is the mean intensity of image y ,
- σ_x^2 is the variance of image x ,
- σ_y^2 is the variance of image y ,
- σ_{xy} is the covariance between images x and y ,
- $C_1 = (K_1 L)^2$,
- $C_2 = (K_2 L)^2$.

Higher SSIM values (closer to 1) indicate a greater structural resemblance between the two images. Since medical images rely heavily on structural integrity for clinical interpretation, SSIM is particularly valuable in evaluating H&E to IHC translations, ensuring that spatial structures are preserved despite color and texture transformations.

3) *Fréchet Inception Distance (FID)*: FID assesses the quality and diversity of the generated images by comparing the statistical distribution of deep features extracted from a pre-trained Inception v3 model [48]. Unlike PSNR and SSIM, which evaluate pixel-wise differences, FID provides a perceptual similarity measure at a higher abstraction level. It is defined as:

$$\text{FID}(P_r, P_g) = \|\mu_r - \mu_g\|^2 + \text{Tr}(\Sigma_r + \Sigma_g - 2(\Sigma_r \Sigma_g)^{1/2}), \quad (14)$$

where:

- μ_r and μ_g are the means of the feature activations for real and generated images, respectively.
- Σ_r and Σ_g are the covariance matrices of the feature activations for real and generated images, respectively.
- Tr denotes the trace of a matrix.

Lower FID values indicate greater similarity between the distributions of real and generated images, reflecting improved realism and diversity in the generated IHC images. In the context of HE to IHC translation, FID ensures that the generated images not only resemble real IHC images in appearance but also capture the statistical properties of real IHC data, which is crucial for clinical applicability.

4) *Summary of Metrics*: A high-quality HE to IHC image translation model should produce images with:

- Higher PSNR values, indicating lower pixel-wise reconstruction error.
- Higher SSIM values, ensuring structural similarity with the ground truth.
- Lower FID values, demonstrating better perceptual realism and diversity.

Using these complementary metrics, we provide a comprehensive evaluation of our model's ability to generate high-fidelity IHC images from H&E-stained input images, ensuring both visual and statistical alignment with real IHC data.

C. Experimental Framework

The BCI dataset [10] we used consists of 4873 paired hematoxylin and eosin (H&E) and HER2 Immunohistochemistry (IHC) stained images. The IHC images are further classified

into four categories based on staining intensity and membrane completeness, which help determine HER2 expression levels in tumor cells. IHC 0 is considered negative, showing no staining or faint, incomplete membrane staining in less than 10% of tumor cells. IHC 1+ is also negative but presents weak and incomplete membrane staining in more than 10% of tumor cells. IHC 2+ is considered equivocal, displaying weak to moderate complete membrane staining in over 10% of tumor cells, often requiring fluorescence in situ hybridization (FISH) for confirmation. IHC 3+, classified as HER2-positive, exhibits strong, circumferential membrane staining in more than 10% of tumor cells, confirming HER2 overexpression without the need for additional testing.

Our method is tested for all four categories and We employ a five-fold cross-validation approach to ensure robustness and mitigate overfitting. The dataset is randomly partitioned into five equal subsets, where in each iteration, four subsets (3898 image pairs) are used for training, and the remaining subset is reserved for testing. This process is repeated five times, with each subset serving as the test set once. The final performance metrics are computed by averaging results across all five folds.

The training dataset comprises images exhibiting diverse characteristics based on HER2 concentration levels, as reflected by variations in statistical properties such as color distribution, sharpness, and dynamic range. These variations are quantitatively illustrated in Figures 7, 8, and 9. To account for these differences, we train our model separately for each category of images.

To evaluate our proposed method, we compare the performance metrics, *Peak Signal-to-Noise Ratio (PSNR)*, *Structural Similarity Index (SSIM)*, and *Fréchet Inception Distance (FID)*, against two baseline methods: *pix2pix* [40] and *pyramid pix2pix* [10]. To optimize computational efficiency, input images are cropped before being fed into the generator.

The generator in our proposed framework utilizes a *ResNet-9blocks* architecture, while the discriminator follows the default *PatchGAN* configuration. Training is conducted with a batch size of 4 for 200 epochs. The optimization is performed using the *Adam* optimizer, with an initial learning rate of 0.0002 for the first 50 epochs, which then linearly decays to zero over the remaining epochs. The momentum parameter for Adam is set to 0.5. The generator is trained using the loss function defined in Equation 10, incorporating our proposed variance-based loss term.

V. RESULTS

To comprehensively assess the effectiveness of our proposed model, we evaluated its performance across multiple classes of images, focusing on its ability to generate high-fidelity immunohistochemistry (IHC) images from hematoxylin and eosin (H&E) stained images. Our results are presented in comparison with state-of-the-art models, including *pix2pix* [40] and *pyramid pix2pix* [10], using the Breast Cancer Immunohistochemistry (BCI) dataset.

A. Evaluation on BCI Dataset for H&E to IHC Translation

To assess the effectiveness of our proposed model in translating hematoxylin and eosin (H&E) stained images into

TABLE I: Comparison of Evaluation Metrics for pix2pix, pyramid pix2pix, and Our Method for IHC 0.

Metrics	pix2pix	pyramid pix2pix	ours
PSNR	19.05	19.43	20.10
SSIM	0.34	0.23	0.32
FID	901.62	1154.80	1185.07

TABLE II: Comparison of Evaluation Metrics for pix2pix, pyramid pix2pix, and Our Method for IHC 1+.

Metrics	pix2pix	pyramid pix2pix	ours
PSNR	19.03	20.06	20.24
SSIM	0.33	0.31	0.29
FID	946.18	921.64	925.24

high-fidelity immunohistochemistry (IHC) images, particularly for HER2-positive (IHC 3+) cases, we performed a detailed quantitative and qualitative analysis. Figures 10-12 illustrate the peak signal-to-noise ratio (PSNR), the structural similarity index (SSIM), and the Fréchet inception distance (FID) between different levels of expression of HER2. Our model consistently demonstrates superior performance, as evident by higher SSIM, PSNR, and lower FID scores, particularly for IHC 3+ images. This confirms that our method enhances the fidelity of IHC image synthesis, addressing the primary challenge of accurately reconstructing HER2-positive cases, which has remained a limitation of previous models.

B. Comparison with Existing Methods on BCI Dataset

The evaluation metrics for our methodology, using the BCI dataset, are presented in comparison with existing approaches, namely pix2pix [40] and pyramid pix2pix [10], in Tables I-IV. Notably, our approach achieves the highest PSNR values across all IHC classes, reflecting improved pixel-level accuracy in the reconstructed images. Simultaneously, we obtain competitive or superior SSIM scores, indicating better preservation of structural details, which is critical for clinical interpretability.

Figure 13 further quantifies the improvements achieved by our model, showing the percentage gain in performance against the pyramid pix2pix model. Our variance-based loss function plays a crucial role in mitigating mode collapse, resulting in a broader diversity of generated images and ensuring that the synthetic IHC images accurately capture the inherent variability observed in real-world HER2-positive

TABLE III: Comparison of Evaluation Metrics for pix2pix, pyramid pix2pix, and Our Method for IHC 2+.

Metrics	pix2pix	pyramid pix2pix	ours
PSNR	18.32	18.81	18.40
SSIM	0.31	0.32	0.30
FID	473.25	466.12	560.55

TABLE IV: Comparison of Evaluation Metrics for pix2pix, pyramid pix2pix, and Our Method for IHC 3+.

Metrics	pix2pix	pyramid pix2pix	ours
PSNR	15.17	16.04	17.50
SSIM	0.251	0.252	0.300
FID	687.83	777.15	683.70

cases. This advancement is critical for reliable computational pathology, where the preservation of fine-grained details in IHC images is paramount for clinical decision-making.

Additionally, Figure 14 presents a qualitative comparison of IHC images generated for various HER2 expression levels using different models. The images generated by our approach more closely resemble the ground truth IHC images across all HER2 classes, with a particularly noticeable improvement for IHC 3+ cases. This substantiates our model’s ability to translate H&E images into realistic IHC representations, reinforcing its utility in medical image analysis and diagnostic workflows.

C. Generalizability: Evaluation on LLVIP Dataset

To evaluate the broader applicability of our model beyond medical imaging, we tested it on the LLVIP dataset [17], a visible-infrared paired dataset designed for low-light vision applications. This dataset comprises 15,488 paired images, enabling a comprehensive assessment of our model’s generalizability in diverse image translation tasks.

Table VI reports the evaluation metrics, demonstrating that our model achieves superior performance compared to state-of-the-art methods in this domain. The ability of our model to generalize effectively to non-medical image-to-image translation tasks highlights its robustness and adaptability, further validating the impact of our variance-based loss function in mitigating mode collapse across different domains.

These findings emphasize the broader significance of our approach, indicating that our model is not only highly effective for H&E to IHC translation but also possesses the versatility to be extended to various image translation applications beyond biomedical imaging.

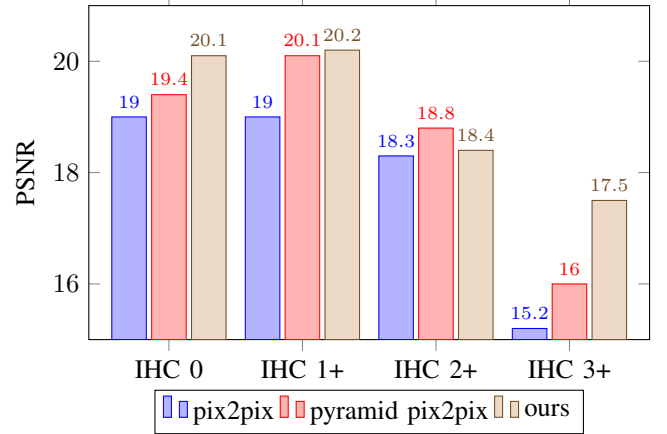


Fig. 10: PSNR Comparison for pix2pix, pyramid pix2pix, and Our Method

VI. DISCUSSION

The challenge of accurately translating hematoxylin and eosin (H&E) stained tissue into immunohistochemistry (IHC) representations, particularly for HER2-positive (IHC 3+) cases, have impeded broader clinical deployment of generative

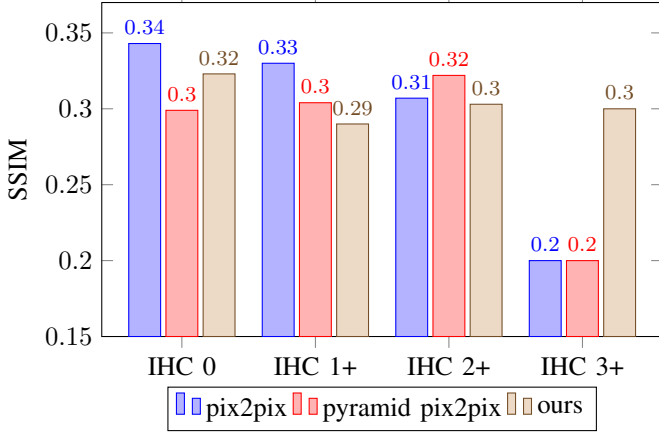


Fig. 11: SSIM Comparison for pix2pix, pyramid pix2pix, and our Method

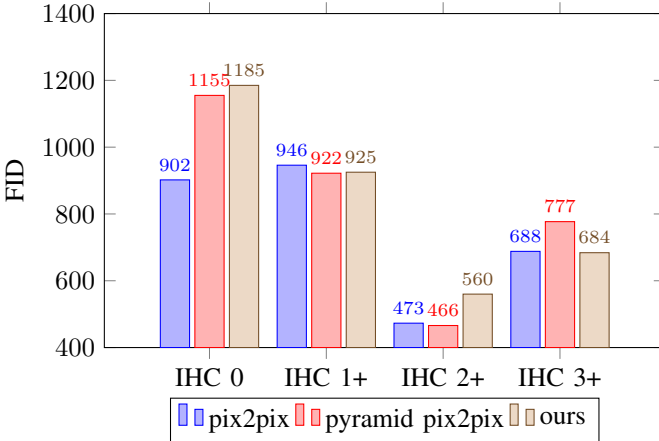


Fig. 12: FID Comparison for pix2pix, pyramid pix2pix, and Our Method

TABLE V: Comparison of Average Evaluation Metrics for pix2pix, pyramid pix2pix and Our Method using BCI dataset

Metric	pix2pix	pyramid pix2pix	ours
PSNR	17.891	18.583	19.056
SSIM	0.307	0.294	0.304
FID	752.22	829.926	838.64

TABLE VI: Comparison of Evaluation Metrics for pyramid pix2pix and Our Method using LLVIP dataset

Metric	pyramid pix2pix	ours
PSNR	12.824	13.16
SSIM	0.3	0.3

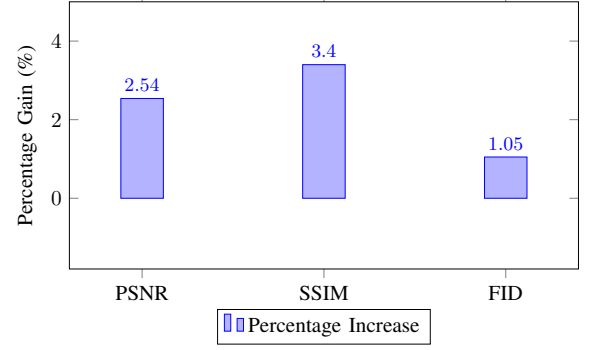


Fig. 13: Percentage Increase for PSNR, SSIM, and FID for our Method

models in digital pathology. Existing frameworks often struggle to preserve fine-grained morphological and phenotypic features critical for accurate biomarker assessment. Our work addresses this long-standing limitation by introducing a novel variance-based penalty term into the pyramid pix2pix architecture, which fundamentally reshapes the loss penalty landscape to encourage diversity and fidelity in the generated images. The proposed modification to the loss function, detailed in eq. 10, effectively addresses the mode collapse problem by introducing a penalty for generating less diverse images. The results affirm the effectiveness of this modification across three pivotal dimensions: improved HER2-positive translation accuracy, mitigation of mode collapse, and generalizability to non-medical image translation tasks.

A. High-Fidelity Translation of HER2-Positive (IHC 3+) Images

HER2-positive tumors, marked by strong circumferential membrane staining, present high morphological heterogeneity that has historically confounded generative models. While prior models such as pix2pix and pyramid pix2pix achieved reasonable performance on low-expression IHC classes (0/1+/2+), they consistently failed to generate realistic IHC 3+ images, a shortcoming with direct clinical implications. By incorporating a variance-based penalty that directly targets the model's tendency toward oversimplified outputs, our method achieves substantial gains in PSNR and SSIM for IHC 3+ cases. Specifically, PSNR improved by over 9% and SSIM by nearly 20% relative to pyramid pix2pix, reflecting enhanced pixel-level fidelity and structural coherence. Crucially, the decrease in Fréchet Inception Distance (FID) for IHC 3+, a metric sensitive to perceptual realism and distributional alignment, demonstrates that our model not only improves quantitative performance but also generates images with higher diagnostic plausibility. As shown in Fig. 14, our method consistently produces more diverse and representative images across different classes of input, particularly in comparison to baseline methods such as pix2pix and pyramid pix2pix.

B. Variance-Based Penalty and Mitigation of Mode Collapse

Mode collapse remains one of the most persistent and debilitating issues in GAN-based translation models, often

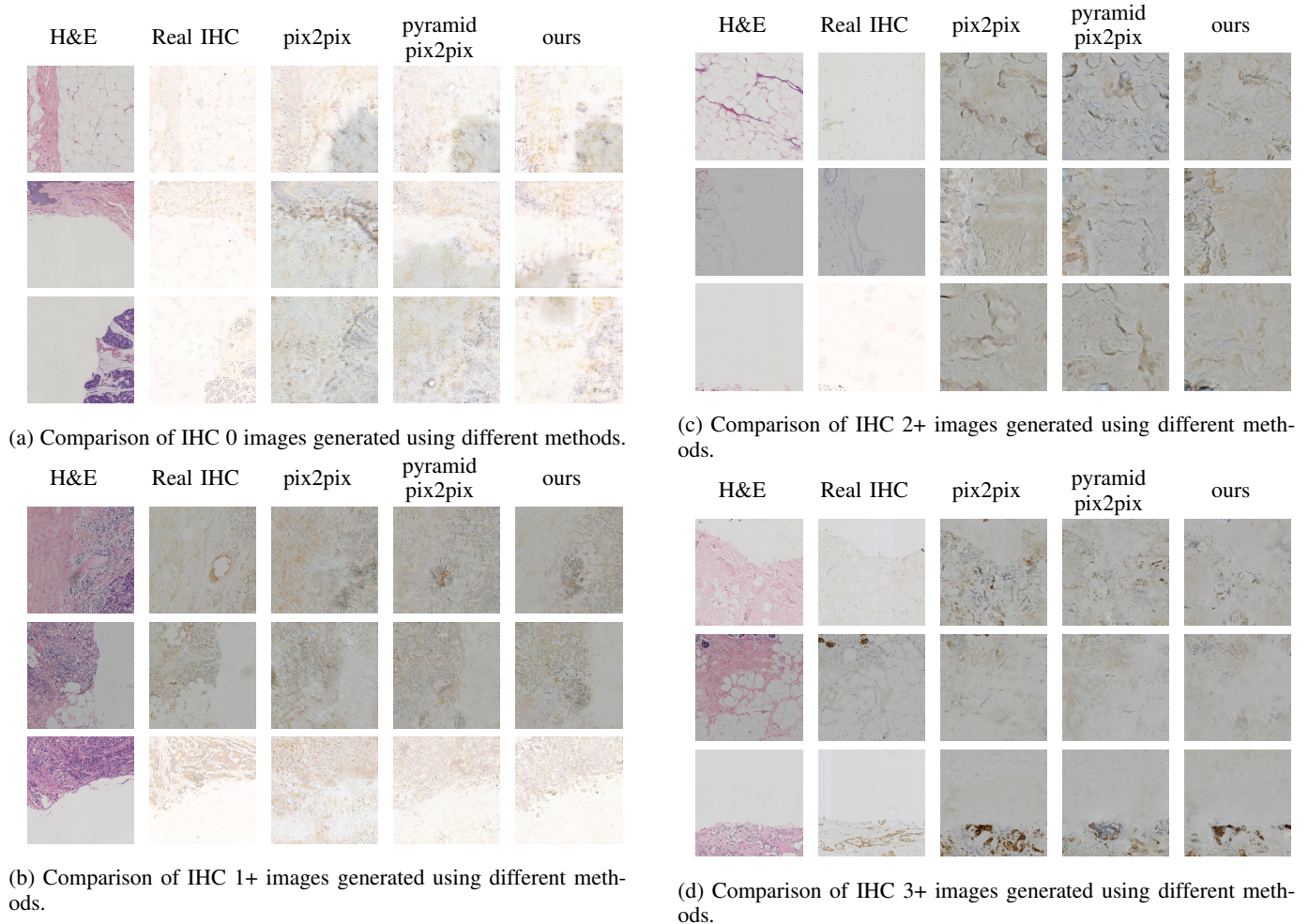


Fig. 14: Comparison of different types of IHC images generated using different methods. The first column shows three randomly chosen input H&E images, the second columns shows the corresponding real IHC images. The third, fourth and fifth columns represent IHC images generated using pix2pix, pyramid pix2pix and our method respectively. The images generated by our method are closer to the real IHC images.

manifesting as repetitive or degenerate outputs. Traditional solutions have explored architectural adjustments or adversarial training stabilization techniques, but few have directly targeted the diversity of outputs through the loss function. Our contribution departs from this paradigm by introducing a batch-level variance regularization term that penalizes the model when the variance in generated images deviates significantly from that of the real distribution. This variance-based constraint acts as a statistical anchor, encouraging the generator to produce outputs that span the intrinsic variability of the target domain.

The empirical results confirm the efficacy of this strategy. Across HER2 classes, our model exhibits higher intra-class variance while maintaining or improving fidelity metrics. This balance between diversity and accuracy is critical, especially in histopathological contexts where subtle phenotypic variations bear diagnostic weight. Our findings suggest that loss-level interventions, particularly those informed by global statistical properties, offer a promising new direction for tackling mode collapse in medically constrained GAN applications.

C. Generalizability Beyond Medical Imaging

The proposed model was initially optimized for histopathological image translation task, we further evaluated its generalization capability on the LLVIP dataset, a benchmark in the domain of visible-to-infrared translation. The ability of our model to outperform pyramid pix2pix in both PSNR and SSIM on this out-of-domain task highlights the robustness and adaptability of our variance-regularized framework. This observation is nontrivial: most domain-specific models overfit to localized feature distributions and exhibit poor transferability. Our results indicate that the variance-based penalty does not merely fine-tune the model for HER2 classification, but rather instills a broader inductive bias toward generative diversity, a quality that enhances performance even in unrelated modalities.

The implications of this work extend beyond technical performance gains. From a clinical standpoint, the improved translation of HER2-positive cases opens avenues for more reliable, cost-effective, and scalable HER2 screening pipelines, especially in low-resource settings where IHC reagents and

pathologist expertise are limited. From a methodological perspective, our findings support a more systemic reconsideration of loss functions in GANs, advocating for principled regularization strategies that reflect underlying statistical properties of the data.

Future work may explore hierarchical or region-specific variance constraints to further tailor the loss function to heterogeneous tissue morphologies. Moreover, integrating uncertainty quantification, through Bayesian or ensemble approaches, could provide valuable confidence estimates, enhancing clinical interpretability and trust. Finally, expanding the model to support multiplexed biomarker generation could transform its utility from a diagnostic aid into a tool for digital pathology simulation and augmentation.

VII. CONCLUSION

This paper suggests changes in the pyramid pix2pix model for translation of high-fidelity IHC images from H&E images. IHC images are used for the detection of HER2 cancer. To reduce the problem of mode collapse in the pyramid pix2pix model, we introduce a term in the objective function of the model that will penalize the model for generating images with relatively less variance with respect to the input images. The proposed model not only outperforms the state-of-the-art models in translation from H&E images to IHC images, it also reports better evaluation scores for generic datasets. In the presence of enough computational resources, the input images do not need to be cropped, which may further improve our results.

VIII. ACKNOWLEDGMENT

The publication of this article was funded by Qatar National Library.

REFERENCES

- [1] S. Lei, R. Zheng, S. Zhang, S. Wang, R. Chen, K. Sun, H. Zeng, J. Zhou, and W. Wei, "Global patterns of breast cancer incidence and mortality: A population-based cancer registry data analysis from 2000 to 2020," *Cancer Communications*, vol. 41, no. 11, pp. 1183–1194, 2021.
- [2] R. L. Siegel, K. D. Miller, H. E. Fuchs, and A. Jemal, "Cancer statistics, 2022," *CA: A Cancer Journal for Clinicians*, vol. 72, no. 1, pp. 7–33, 2022.
- [3] D. J. Slamon, G. M. Clark, S. G. Wong, W. J. Levin, A. Ullrich, and W. L. McGuire, "Human breast cancer: correlation of relapse and survival with amplification of the her-2/neu oncogene," *science*, vol. 235, no. 4785, pp. 177–182, 1987.
- [4] R. Prati, S. K. Apple, J. He, J. A. Gornbein, and H. R. Chang, "Histopathologic characteristics predicting her-2/neu amplification in breast cancer," *The breast journal*, vol. 11, no. 6, pp. 433–439, 2005.
- [5] J. S. Ross, J. A. Fletcher, K. J. Bloom, G. P. Linette, J. Stec, W. F. Symmans, L. Pusztai, and G. N. Hortobagyi, "Targeted therapy in breast cancer: the her-2/neu gene and protein," *Molecular & Cellular Proteomics*, vol. 3, no. 4, pp. 379–398, 2004.
- [6] T. A. Thomson, M. M. Hayes, J. J. Spinelli, E. Hilland, C. Sawrenko, D. Phillips, B. Dupuis, and R. L. Parker, "Her-2/neu in breast cancer: interobserver variability and performance of immunohistochemistry with 4 antibodies compared with fluorescent in situ hybridization," *Modern Pathology*, vol. 14, no. 11, pp. 1079–1086, 2001.
- [7] M. Van de Vijver, "Assessment of the need and appropriate method for testing for the human epidermal growth factor receptor-2 (her2)," *European Journal of cancer*, vol. 37, pp. 11–17, 2001.
- [8] J. A. Robb, L. Bry, P. M. Sluss, E. A. Wagar, M. F. Kennedy, C. of American Pathologists Diagnostic Intelligence, and H. I. T. B. W. G. 2, "A call to standardize preanalytic data elements for biospecimens, part ii," *Archives of Pathology and Laboratory Medicine*, vol. 139, no. 9, pp. 1125–1128, 2015.
- [9] F. Lin and Z. Chen, "Standardization of diagnostic immunohistochemistry: literature review and geisinger experience," *Archives of Pathology & Laboratory Medicine*, vol. 138, no. 12, pp. 1564–1577, 2014.
- [10] S. Liu, C. Zhu, F. Xu, X. Jia, Z. Shi, and M. Jin, "Bci: Breast cancer immunohistochemical image generation through pyramid pix2pix," in *Proceedings of the IEEE/CVF Conference on Computer Vision and Pattern Recognition*, 2022, pp. 1815–1824.
- [11] G. Shama, Y. Binenbaum, R. Slossberg, I. Duek, Z. Gil, and R. Kimmel, "Artificial intelligence algorithms to assess hormonal status from tissue microarrays in patients with breast cancer," *JAMA network open*, vol. 2, no. 7, pp. e197700–e197700, 2019.
- [12] P. Gamble, R. Jaroensri, H. Wang, F. Tan, M. Moran, T. Brown, I. Flament-Auvigne, E. A. Rakha, M. Toss, D. J. Dabbs *et al.*, "Determining breast cancer biomarker status and associated morphological features using deep learning," *Communications medicine*, vol. 1, no. 1, p. 14, 2021.
- [13] N. Naik, A. Madani, A. Esteva, N. S. Keskar, M. F. Press, D. Ruderman, D. B. Agus, and R. Socher, "Deep learning-enabled breast cancer hormonal receptor status determination from base-level h&e stains," *Nature communications*, vol. 11, no. 1, p. 5727, 2020.
- [14] D. Bychkov, N. Linder, A. Tiulpin, H. Kucukel, M. Lundin, S. Nordling, H. Sihto, J. Isola, T. Lehtimäki, P.-L. Kellokumpu-Lehtinen *et al.*, "Deep learning identifies morphological features in breast cancer predictive of cancer erbb2 status and trastuzumab treatment efficacy," *Scientific reports*, vol. 11, no. 1, pp. 1–10, 2021.
- [15] R. R. Rawat, I. Ortega, P. Roy, F. Sha, D. Shibata, D. Ruderman, and D. B. Agus, "Deep learned tissue "fingerprints" classify breast cancers by er/pr/her2 status from h&e images," *Scientific reports*, vol. 10, no. 1, pp. 1–13, 2020.
- [16] J. J. Levy, C. R. Jackson, A. Sriharan, B. C. Christensen, and L. J. Vaickus, "Preliminary evaluation of the utility of deep generative histopathology image translation at a mid-sized nci cancer center," *bioRxiv*, pp. 2020–01, 2020.
- [17] X. Jia, C. Zhu, M. Li, W. Tang, and W. Zhou, "Llvp: A visible-infrared paired dataset for low-light vision," in *Proceedings of the IEEE/CVF international conference on computer vision*, 2021, pp. 3496–3504.
- [18] H. Xu, C. Lu, and M. Mandal, "An efficient technique for nuclei segmentation based on ellipse descriptor analysis and improved seed detection algorithm," *IEEE journal of biomedical and health informatics*, vol. 18, no. 5, pp. 1729–1741, 2014.
- [19] H. Wang, B. Zheng, S. W. Yoon, and H. S. Ko, "A support vector machine-based ensemble algorithm for breast cancer diagnosis," *European Journal of Operational Research*, vol. 267, no. 2, pp. 687–699, 2018.
- [20] V. Kumar, B. K. Mishra, M. Mazzara, D. N. Thanh, and A. Verma, "Prediction of malignant and benign breast cancer: A data mining approach in healthcare applications," in *Advances in Data Science and Management: Proceedings of ICDSM 2019*. Springer, 2020, pp. 435–442.
- [21] V. Lahoura, H. Singh, A. Aggarwal, B. Sharma, M. A. Mohammed, R. Damaševičius, S. Kadry, and K. Cengiz, "Cloud computing-based framework for breast cancer diagnosis using extreme learning machine," *Diagnostics*, vol. 11, no. 2, p. 241, 2021.
- [22] I. Hirra, M. Ahmad, A. Hussain, M. U. Ashraf, I. A. Saeed, S. F. Qadri, A. M. Alghamdi, and A. S. Alfakheh, "Breast cancer classification from histopathological images using patch-based deep learning modeling," *IEEE Access*, vol. 9, pp. 24 273–24 287, 2021.
- [23] Y. Jiang, L. Chen, H. Zhang, and X. Xiao, "Breast cancer histopathological image classification using convolutional neural networks with small se-resnet module," *PloS one*, vol. 14, no. 3, p. e0214587, 2019.
- [24] S. Khan, N. Islam, Z. Jan, I. U. Din, and J. J. C. Rodrigues, "A novel deep learning based framework for the detection and classification of breast cancer using transfer learning," *Pattern Recognition Letters*, vol. 125, pp. 1–6, 2019.
- [25] J. Xie, R. Liu, J. Luttrell, and C. Zhang, "Deep learning based analysis of histopathological images of breast cancer," *Frontiers in genetics*, vol. 10, p. 426920, 2019.
- [26] A. Dosovitskiy, L. Beyer, A. Kolesnikov, D. Weissenborn, X. Zhai, T. Unterthiner, M. Dehghani, M. Minderer, G. Heigold, S. Gelly *et al.*, "An image is worth 16x16 words: Transformers for image recognition at scale," *arXiv preprint arXiv:2010.11929*, 2020.

- [27] H. Touvron, M. Cord, M. Douze, F. Massa, A. Sablayrolles, and H. Jégou, "Training data-efficient image transformers & distillation through attention," in *International conference on machine learning*. PMLR, 2021, pp. 10 347–10 357.
- [28] Z. Liu, Y. Lin, Y. Cao, H. Hu, Y. Wei, Z. Zhang, S. Lin, and B. Guo, "Swin transformer: Hierarchical vision transformer using shifted windows," in *Proceedings of the IEEE/CVF international conference on computer vision*, 2021, pp. 10 012–10 022.
- [29] A. Alotaibi, T. Alafif, F. Alkhilaiwi, Y. Alatawi, H. Althobaiti, A. Al-refaei, Y. Hawsawi, and T. Nguyen, "Vit-deit: An ensemble model for breast cancer histopathological images classification," in *2023 1st International Conference on Advanced Innovations in Smart Cities (ICAISC)*. IEEE, 2023, pp. 1–6.
- [30] S. Tummala, J. Kim, and S. Kadry, "Breast-net: Multi-class classification of breast cancer from histopathological images using ensemble of swin transformers," *Mathematics*, vol. 10, no. 21, p. 4109, 2022.
- [31] Z. Shao, H. Bian, Y. Chen, Y. Wang, J. Zhang, X. Ji *et al.*, "Transmil: Transformer based correlated multiple instance learning for whole slide image classification," *Advances in neural information processing systems*, vol. 34, pp. 2136–2147, 2021.
- [32] A. G. Gul, O. Cetin, C. Reich, N. Flinner, T. Prangemeier, and H. Koeppl, "Histopathological image classification based on self-supervised vision transformer and weak labels," in *Medical Imaging 2022: Digital and Computational Pathology*, vol. 12039. SPIE, 2022, pp. 366–373.
- [33] W. Wang, R. Jiang, and Z. Xiao, "Semi-supervised vision transformer with adaptive token sampling for breast cancer classification," *Frontiers in Pharmacology*, vol. 13, p. 929755, 2022.
- [34] F. A. Spanhol, L. S. Oliveira, C. Petitjean, and L. Heutte, "A dataset for breast cancer histopathological image classification," *Ieee transactions on biomedical engineering*, vol. 63, no. 7, pp. 1455–1462, 2015.
- [35] A. Aksac, D. J. Demetrick, T. Ozyer, and R. Alhaji, "Brecahad: a dataset for breast cancer histopathological annotation and diagnosis," *BMC research notes*, vol. 12, pp. 1–3, 2019.
- [36] G. Aresta, T. Araújo, S. Kwok, S. S. Chennamsetty, M. Safwan, V. Alex, B. Marami, M. Prastawa, M. Chan, M. Donovan *et al.*, "Bach: Grand challenge on breast cancer histology images," *Medical image analysis*, vol. 56, pp. 122–139, 2019.
- [37] J.-Y. Zhu, T. Park, P. Isola, and A. A. Efros, "Unpaired image-to-image translation using cycle-consistent adversarial networks," in *Proceedings of the IEEE international conference on computer vision*, 2017, pp. 2223–2232.
- [38] Z. Yi, H. Zhang, P. Tan, and M. Gong, "Dualgan: Unsupervised dual learning for image-to-image translation," in *Proceedings of the IEEE international conference on computer vision*, 2017, pp. 2849–2857.
- [39] M.-Y. Liu, T. Breuel, and J. Kautz, "Unsupervised image-to-image translation networks," *Advances in neural information processing systems*, vol. 30, 2017.
- [40] P. Isola, J.-Y. Zhu, T. Zhou, and A. A. Efros, "Image-to-image translation with conditional adversarial networks," in *Proceedings of the IEEE conference on computer vision and pattern recognition*, 2017, pp. 1125–1134.
- [41] T.-C. Wang, M.-Y. Liu, J.-Y. Zhu, A. Tao, J. Kautz, and B. Catanzaro, "High-resolution image synthesis and semantic manipulation with conditional gans," in *Proceedings of the IEEE conference on computer vision and pattern recognition*, 2018, pp. 8798–8807.
- [42] J. Adler and S. Lunz, "Banach wasserstein gan," *Advances in neural information processing systems*, vol. 31, 2018.
- [43] T. Miyato, T. Kataoka, M. Koyama, and Y. Yoshida, "Spectral normalization for generative adversarial networks," *arXiv preprint arXiv:1802.05957*, 2018.
- [44] T. Che, Y. Li, A. P. Jacob, Y. Bengio, and W. Li, "Mode regularized generative adversarial networks," *arXiv preprint arXiv:1612.02136*, 2016.
- [45] H. Zhang, I. Goodfellow, D. Metaxas, and A. Odena, "Self-attention generative adversarial networks," in *International conference on machine learning*. PMLR, 2019, pp. 7354–7363.
- [46] Z. Wang, A. C. Bovik, H. R. Sheikh, and E. P. Simoncelli, "Image quality assessment: from error visibility to structural similarity," *IEEE transactions on image processing*, vol. 13, no. 4, pp. 600–612, 2004.
- [47] M. Heusel, H. Ramsauer, T. Unterthiner, B. Nessler, and S. Hochreiter, "Gans trained by a two time-scale update rule converge to a local nash equilibrium," *Advances in neural information processing systems*, vol. 30, 2017.
- [48] C. Szegedy, V. Vanhoucke, S. Ioffe, J. Shlens, and Z. Wojna, "Rethinking the inception architecture for computer vision," in *Proceedings of the IEEE conference on computer vision and pattern recognition*, 2016, pp. 2818–2826.